Physica B 175 (1991) 412–434
North-Holland

PHYSICA B

Generalised Langevin–Kielich functions for the optical Kerr effect in liquid water: theory and simulation

M.W. Evans[1], S. Woźniak[2] and G. Wagnière

Institute of Physical Chemistry, University of Zurich, Winterthurerstrasse 190, CH 8057 Zurich, Switzerland

Received 2 April 1991

A field applied molecular dynamics (FMD) computer simulation of the optical Kerr effect in liquid water has produced femtosecond rise transients, the final levels of which accurately reproduce a new theoretical treatment based on generalised Langevin–Kielich functions for the asymmetric top. The transients and associated field applied correlation functions prove to be sensitive to the anisotropy of polarisability (δ) in water, showing that femtosecond transient spectroscopy is potentially a much more accurate method of measurement of the anisotropy of polarisability than hitherto available. Generalised Langevin–Kielich functions are presented as a function of both the anisotropies of polarisability (γ and δ) of the asymmetric top in a form suitable for use in other contexts, such as light scattering in the presence of a strong electric field. For three literature estimates of γ, the laser-on steady state molecular dynamics of water are investigated in terms of a range of time correlation functions, the results being significantly different for each estimate.

1. Introduction

The optical Kerr effect is well known to be observable as the rotation of the plane of polarisation of a linearly polarised probe laser due to a pulse of powerful pump laser radiation, linearly polarised in the X-axis of the laboratory frame. It is a phenomenon of four wave mixing, and provides information on the anisotropy of molecular polarisability. The optical Kerr effect (OKE) was first investigated in time averaged pump laser applied states, and rapid developments in the last decade now allow observation of transient phenomena associated with the OKE with a femtosecond time resolution. The transient observable is usually a change in power absorption coefficient due to a pump laser pulse, which is related through the Kramers–Kronig equation to a transient birefringence.

In this paper we report the first computer simulation of the optical Kerr effect, using field applied molecular dynamics (FMD). FMD is a simple variation on standard molecular dynamics computer simulation in which the torque generated between the molecules of an ensemble and an external field is coded into the forces loop. FMD provides rise and fall transients, thermodynamic and structural data, and field on or field free statistical mechanical data, for example time correlation functions of many different kinds [1], some of which are Fourier transforms of directly observable spectra. FMD was devised originally for strong electric fields, and accurately reproduced known Langevin and Kielich functions [2–4] from the final levels of rise transients. Additionally, it gave details of the time resolution of the transients themselves on the femto/picosecond scale, information which is now becoming directly accessible experimentally [5] in the transient optical Kerr effect. FMD also gives a wealth of information from the same trajectories on the dynamics of the laser-applied steady state in the optical Kerr effect, on fall transients [6–8], and on pair distribution functions [9]. The method was later

[1] Permanent address: 433 Theory Center, Cornell University, Ithaca, NY 14853, USA.
[2] Permanent address: Non-linear Optics Division, Collegium Physicum, Adam Mickiewicz University, 60–780 Poznań, Poland.

extended for use with circularly polarised laser fields [10, 11], and for non-linear optical phenomena where in general [12–14], a laser field or field gradient forms a torque with an induced electric or magnetic dipole or multipole. FMD also revealed basic statistical mechanical laws such as fall transient acceleration [15], field decoupling [15], and rise transient oscillations on the femtosecond scale [16, 17]; its generality springs from the fact that the integral of the torque with respect to orientation is potential energy, a term which is added to the Hamiltonian as the starting point of analytical theory. The interaction of any type of field and any type of ensemble is therefore described at a fundamental level, as in semi-classical theory [18], but FMD provides additionally much more information from the same set of molecular trajectories.

The particular type of torque relevant to the optical Kerr effect is described in section 2. The essentials of FMD in this context are recounted briefly in section 3, followed in section 4 by a description of second order rise transients and a comparison with generalised n order Langevin–Kielich functions for the asymmetric top molecule. The latter from both simulation and theory are shown in two cases to change direction (i.e. fall rather than rise from an initial value of $\frac{1}{3}$), with change of sign of the anisotropy of polarisability (δ), thus providing a potentially accurate method of measurement of this quantity in water from the transient optical Kerr effect [5]. Detailed agreement is demonstrated between simulation and theory concerning this useful change of direction and other transient properties of the optical Kerr effect. Section 5 details the time resolution of the rise transients from FMD for three different literature estimates of the second anisotropy of polarisability γ of the water molecule. Section 6 presents a set of generalised Langevin–Kielich functions for the asymmetric top molecule in terms of the anisotropy ratio h/q. These curves are generally useful for a range of phenomena, and are given in terms of Φ, R and K functions, the former being two components of the birefringence, which is proportional to K. The anisotropy ratio h/q varies from 0.25 to 20, giving a wide variety of analytical behaviour pertinent to the optical Kerr effect and several other phenomena. Finally section 7 presents a statistical dynamics analysis of time correlation functions from the FMD simulation in the pump laser applied steady state for the three literature estimates of anisotropy of polarisability, revealing significant differences. There is a need therefore to define much more precisely the anisotropy of polarisability of water and asymmetric tops in general.

2. Torque of the optical Kerr effect

Since its first experimental demonstration by Mayer and Gires [19] the optical Kerr effect has been incisive in the investigation of the optical properties of molecular systems [20–24]. The effect is due to two fundamental mechanisms: (i) the charge distribution in the molecule is modified by the external optical pump beam, thus affecting the hyperpolarisability [25], and (ii) the molecules are reoriented by the field. The latter mechanism dominates for anisotropic molecules [21].

The electric field $\boldsymbol{E}$ of the pump laser beam induces in a molecule an electric dipole moment

$$\boldsymbol{\mu} = \boldsymbol{\alpha} \cdot \boldsymbol{E} , \tag{1}$$

and a time independent torque

$$\boldsymbol{T} = -\boldsymbol{\mu} \times \boldsymbol{E}^* = -(\boldsymbol{\alpha} \cdot \boldsymbol{E}) \times \boldsymbol{E}^* , \tag{2}$$

where $\boldsymbol{\alpha}$ is the complex, second rank, electronic polarisability tensor, defined through electric dipole transitions. We consider the field $\boldsymbol{E}$ linearly polarised in the X-axis of the laboratory frame (X, Y, Z). In the most general case, there are three different components of the molecular polarisability

$\alpha(\alpha_{11} \neq \alpha_{22} \neq \alpha_{33})$, and we have the following expression for the torque (2) in the frame (1, 2, 3) of the principal molecular moments of inertia

$$\begin{aligned} T_1 &= e_{2X}e_{3X}(\alpha_{33} - \alpha_{22})E_0^2 , \\ T_2 &= e_{1X}e_{3X}(\alpha_{11} - \alpha_{33})E_0^2 , \\ T_3 &= e_{1X}e_{2X}(\alpha_{22} - \alpha_{11})E_0^2 , \end{aligned} \tag{3}$$

where $E_0^2 \equiv EE^*$ and the quantities e_{1X}, e_{2X}, and e_{3X} are X components of the unit vectors in axes 1, 2, and 3. Here 1 is the dipole axis, and 2 and 3 are mutually orthogonal in a right-hand frame.

It is assumed that the polarisability is diagonalised in the same frame (1, 2, 3), giving the diagonal components α_{11}, α_{22}, and α_{33} of the molecular polarisability of water. It is convenient in this context to define the two anisotropies of polarisability of the asymmetric top water molecule

$$\gamma = \alpha_{11} - \tfrac{1}{2}(\alpha_{22} + \alpha_{33}) , \tag{4}$$

$$\delta = \tfrac{1}{2}(\alpha_{22} - \alpha_{33}) . \tag{5}$$

The torque components (3) can be coded, in general, into the forces loop of any MD algorithm, and back transformed [14] into the laboratory frame (X, Y, Z) using a rotation matrix

$$\begin{bmatrix} T_X \\ T_Y \\ T_Z \end{bmatrix} = \begin{bmatrix} e_{1X} & e_{2X} & e_{3X} \\ e_{1Y} & e_{2Y} & e_{3Y} \\ e_{1Z} & e_{2Z} & e_{3Z} \end{bmatrix} \begin{bmatrix} T_1 \\ T_2 \\ T_3 \end{bmatrix} . \tag{6}$$

The MD algorithm essentially works out the influence of the torque on various molecular dynamical variables and integrates the torque over configuration space to give potential energy, i.e. an additional term in the Hamiltonian.

3. FMD method

The FMD method was implemented with a sample of 108 water molecules interacting through a modified ST2 potential using Lennard–Jones and partial charge interactions

$$\begin{aligned} &\phi_{ij}(r_i, r_j) = 4\epsilon\left[\left(\frac{\sigma}{r_{ij}}\right)^{12} - \left(\frac{\sigma}{r_{ij}}\right)^{6}\right] + \text{charge–charge} , \\ &\phi_{ij} = \sum\sum \phi_{ij}(\text{site}) , \\ &\epsilon/k(\text{H–H}) = 21.1\ \text{K} , \qquad \sigma(\text{H–H}) = 2.25\ \text{Å} \\ &\epsilon/k(\text{O–O}) = 58.4\ \text{K} , \qquad \sigma(\text{O–O}) = 2.80\ \text{Å} , \\ &q_{\text{H}} = 0.23|e| , \qquad q(\text{lone pair}) = -0.23|e| , \\ &q_{\text{O}} = 0.00|e| , \qquad \sigma(\text{O–H}) = \tfrac{1}{2}[\sigma(\text{O–O}) + \sigma(\text{H–H})] , \\ &\epsilon/k(\text{O–H}) = [\epsilon/k(\text{O–O})\epsilon/k(\text{H–H})]^{1/2} . \end{aligned}$$

This potential has been compared in the literature [26] with the ab initio MCYL, and with experimental

data [27] over a wide range of conditions. We stress that FMD can be used with any type of model or ab initio water potential, and any type of MD algorithm. With a time step of 0.5 fs, transients were evaluated for different E_0^2, over a number of time steps sufficient for attainment of the final level, which was measured and used (with uncertainty bars) to construct generalised Langevin–Kielich functions (section 4) by FMD. The latter were also evaluated analytically [28–32]. The transient generating stage was followed by FMD evaluation of statistical dynamical properties in the pump laser applied steady state, using running time averaging over a minimum of 6000 steps. A data bank of many different examples was collected and used to characterise the field-on dynamics (section 7).

Simulations were carried out at 296 K, 1.0 bar in the liquid state of water.

4. Rise transients and anisotropy of polarisability

There have been numerous reports [33–39] of the anisotropy function γ of water. Khanarian and Kent [34] have made a tabular comparison of experimental and ab initio estimates from various sources, six of whose entries were positive, and four negative. In this section we use three literature estimates of the diagonalised polarisability components of water and compare for each generalised Langevin–Kielich functions and time resolved rise transients from FMD and the available theory. The literature estimates used for the analysis are given in table 1. We note that the experimental estimates in this table give a negative anisotropy γ [33], and what is apparently a conflicting positive anisotropy γ [34]. We also use one ab initio result [35].

For each of these three data sets transients and generalised Langevin–Kielich functions (GLKs) were simulated for $\langle e_{1X}^n \rangle$, $\langle e_{2X}^n \rangle$, and $\langle e_{3X}^n \rangle$, where $n = 2, 4, 6$. GLKs were also evaluated analytically [28–32] from the following theory of the Langevin–Kielich functions. The time independent potential energy of a molecule in the presence of the electric field $\boldsymbol{E}$ of the pump laser

$$U = -\tfrac{1}{2}\alpha_{ij}E_iE_j^* - \tfrac{1}{2}\alpha_{ij}^*E_i^*E_j\,, \tag{7}$$

can be expressed through the anisotropies (4) and (5) and the mean value of the polarisability $\boldsymbol{\alpha}$ ($\alpha = \frac{1}{3}(\alpha_{11} + \alpha_{22} + \alpha_{33})$):

$$U = -(\alpha + \delta(e_{aX}^2 - e_{3X}^2) + \gamma(e_{1X}^2 - \tfrac{1}{3}))E_0^2\,. \tag{8}$$

Denoting by θ the angle between axis 1 of the molecular frame (1, 2, 3) and the axis X of the laboratory

Table 1
Literature estimates of the polarisability tensor of water diagonalised in (1, 2, 3).
Note carefully that the frame definitions of α_{22} and α_{33} in ref. [34] appear to be opposite to those of refs. [33] and [35]. The numbers below were used throughout in our simulation and analysis, and also as a convenient demonstration of how changing from negative to positive anisotropy affects the nature of GLKs, both in the simulation and in the analytical theory, the integrals (9)–(11) of the text.

Ref.	α_{11}	α_{22}	α_{33}	
[33, 37]	9.62	9.26	10.01	(a.u.)
[34]	1.69	1.9	1.3	(SI units)
[35]	8.15	7.12	9.03	(a.u.)

frame (X, Y, Z), the axis of the electric field E of the linearly polarised laser beam, we have, for Euler's azimuth angle ϕ:

$$\langle e_{1X}^n \rangle = \frac{\int_0^{\pi} \left(\cos^n\theta \exp(q\cos^2\theta) \int_0^{2\pi} \exp(-h\sin^2\theta\cos 2\phi)\,\mathrm{d}\phi \right) \sin\theta\,\mathrm{d}\theta}{\int_0^{\pi} \left(\exp(q\cos^2\theta) \int_0^{2\pi} \exp(-h\sin^2\theta\cos 2\phi)\,\mathrm{d}\phi \right) \sin\theta\,\mathrm{d}\theta} \equiv L_n(q,h)\,, \tag{9}$$

$$\langle e_{2X}^n \rangle = \frac{\int_0^{\pi} \left(\sin^n\theta \exp(q\cos^2\theta) \int_0^{2\pi} \sin^n\phi \exp(-h\sin^2\theta\cos 2\phi)\,d\phi \right) \sin\theta\,\mathrm{d}\theta}{\int_0^{\pi} \left(\exp(q\cos^2\theta) \int_0^{2\pi} \exp(-h\sin^2\theta\cos 2\phi)\,\mathrm{d}\phi \right) \sin\theta\,\mathrm{d}\theta} \equiv L_n^{(1)}(q,h)\,, \tag{10}$$

$$\langle e_{3X}^n \rangle = \frac{\int_0^{\pi} \left(\sin^n\theta \exp(q\cos^2\theta) \int_0^{2\pi} \cos^n\phi \exp(-h\sin^2\theta\cos 2\phi)\,\mathrm{d}\phi \right) \sin\theta\,\mathrm{d}\theta}{\int_0^{\pi} \left(\exp(q\cos^2\theta) \int_0^{2\pi} \exp(-h\sin^2\theta\cos 2\phi)\,\mathrm{d}\phi \right) \sin\theta\,\mathrm{d}\theta} \equiv L_n^{(2)}(q,h)\,, \tag{11}$$

where $L_n(q, h)$, $L_n^{(1)}(q, h)$, and $L_n^{(2)}(q, h)$ may appropriately be named the generalised Langevin–Kielich (GLK) functions. Here

$$q = \gamma E_0^2/kT\,, \quad h = \delta E_0^2/kT\,. \tag{12}$$

If the anisotropy $\delta = 0$, we have

$$L_n(q, h=0) \equiv L_n(q)\,,$$

being the well-known Langevin–Kielich functions [2, 28–32] and

$$L_n^{(1)}(q) = L_n^{(2)}(q) = \langle (1-\cos^2\theta)^{n/2} \rangle \langle \cos^n\phi \rangle\,, \tag{13}$$

with [41]

$$\langle \cos^n\phi \rangle = \langle \sin^n\phi \rangle = \begin{cases} \dfrac{(2t-1)!!}{2^t t!}\,, & n = 2t\,, \\ 0\,, & n = 2t+1\,, \end{cases} \tag{14}$$

and the even order Langevin–Kielich functions $L_{2t} = \langle \cos^{2t}\theta \rangle$. In particular,

$$L_2^{(1)}(q) = L_2^{(2)}(q) = \tfrac{1}{2}(1 - L_2(q))\,, \tag{15}$$

$$L_4^{(1)}(q) = L_4^{(2)}(q) = \tfrac{3}{8}(1 - 2L_2(q) + L_4(q))\,, \tag{16}$$

$$L_6^{(1)}(q) = L_6^{(2)}(q) = \tfrac{5}{16}(1 - 3L_2(q) + 3L_4(q) - L_6(q))\,, \tag{17}$$

and so on, and

$$L_{2t+1}(q) = L^{(1)}_{2t+1}(q) = L^{(2)}_{2t+1}(q) = 0 .$$

The double integrals (9) to (11) were evaluated numerically using IBM software [40] based on accurate fine grid double Gauss Legendre quadrature on the IBM 3090 supercomputer of ETH Zurich. In addition to the special case of water, a set of generalised Langevin–Kielich functions was evaluated numerically in terms of the ratio h/q of the two asymmetric top anisotropies of polarisability, and presented as functions of $|q|$. Each curve of this set required the computation of some eight hundred double integrals. Three curves were usually completed in about 5 min of CPU time.

Figure 1, for the special case of water, illustrates the fact that two of these GLK functions change direction with anisotropy of polarisability δ, in the sense that they increase or decrease from an initial value. Points on these analytical GLKs show simulated data from FMD under the same conditions, with potential energy corresponding to the torque (3) computed over a minimum of 6000 time steps at each point. In matching the analytical curves (obtained by numerical quadrature) with the FMD points, one FMD point, corresponding to a given laser intensity, was matched precisely with the curve, and others added from simulations with different equivalent laser intensities incorporated via the torque. The FMD method successfully simulates the change of direction in $\langle e^n_{2X} \rangle$ and $\langle e^n_{3X} \rangle$ given analytically from (10) and (11) and 2δ is changed from positive to negative for a given γ. The function $\langle e^n_{1X} \rangle$ changes sign analytically as δ/γ increases in eq. (9), except for a very small "blip" at the beginning of its range,

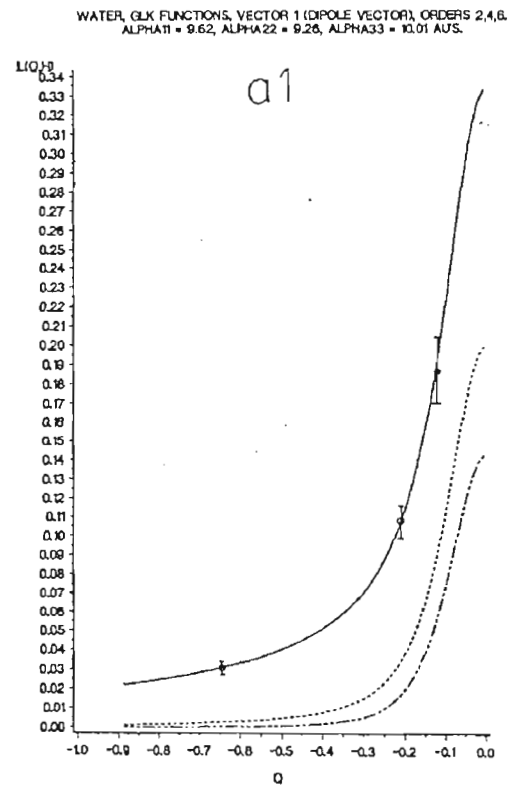

Fig. 1. Generalised Langevin–Kielich functions $L_n(q, h)$; $L^{(1)}_n(q, h)$, and $L^{(2)}_n(q, h)$ from analytical theory (curves) and field applied computer simulation (points) for liquid water at 293 K, 1.0 bar. (a) Using the data (table 1) of ref. [33], (b) ref. [34], (c) ref. [35]. The functions initiate at ⅓ ($n = 2$), ⅕ ($n = 4$), and ⅐ ($n = 6$). Note that in two cases the GLKs change sign between data sets (a) and (b), respectively representing negative and positive γ. ———, $n = 2$; ----, $n = 4$; – · – $n = 6$; ⧳, FMD, $n = 2$.

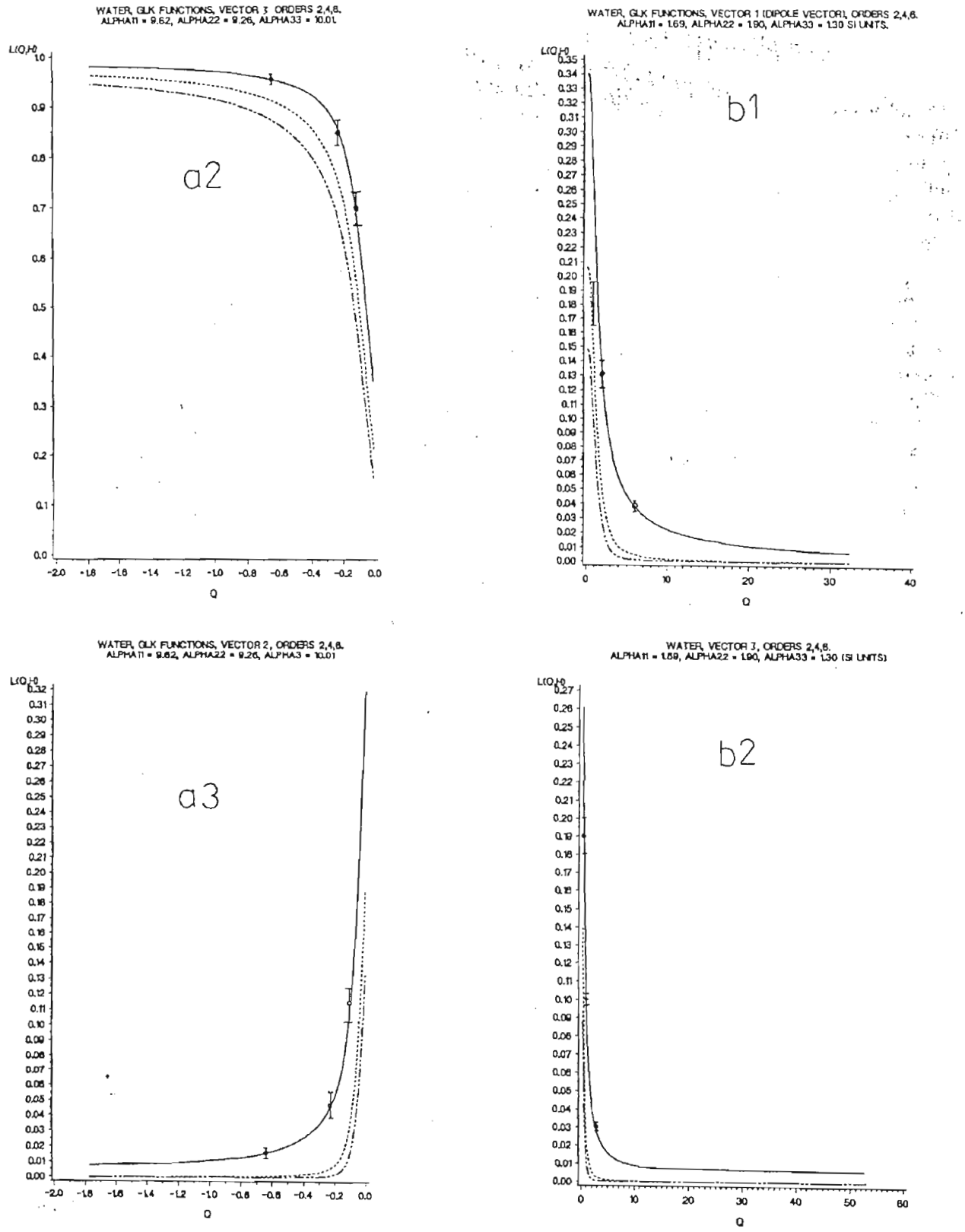
WATER, GLK FUNCTIONS, VECTOR 3 ORDERS 2,4,6.
ALPHA11 = 9.62, ALPHA22 = 9.26, ALPHA33 = 10.01
L(Q)-0
a2
Q
WATER, GLK FUNCTIONS, VECTOR 1 (DIPOLE VECTOR), ORDERS 2,4,6.
ALPHA11 = 1.69, ALPHA22 = 1.90, ALPHA33 = 1.30 SI UNITS.
L(Q)-0
b1
Q
WATER, GLK FUNCTIONS, VECTOR 2, ORDERS 2,4,6.
ALPHA11 = 9.62, ALPHA22 = 9.26, ALPHA3 = 10.01
L(Q)-0
a3
Q
WATER, VECTOR 3, ORDERS 2,4,6.
ALPHA11 = 1.69, ALPHA22 = 1.90, ALPHA33 = 1.30 (SI UNITS)
L(Q)-0
b2
Q

Fig. 1 (cont.).

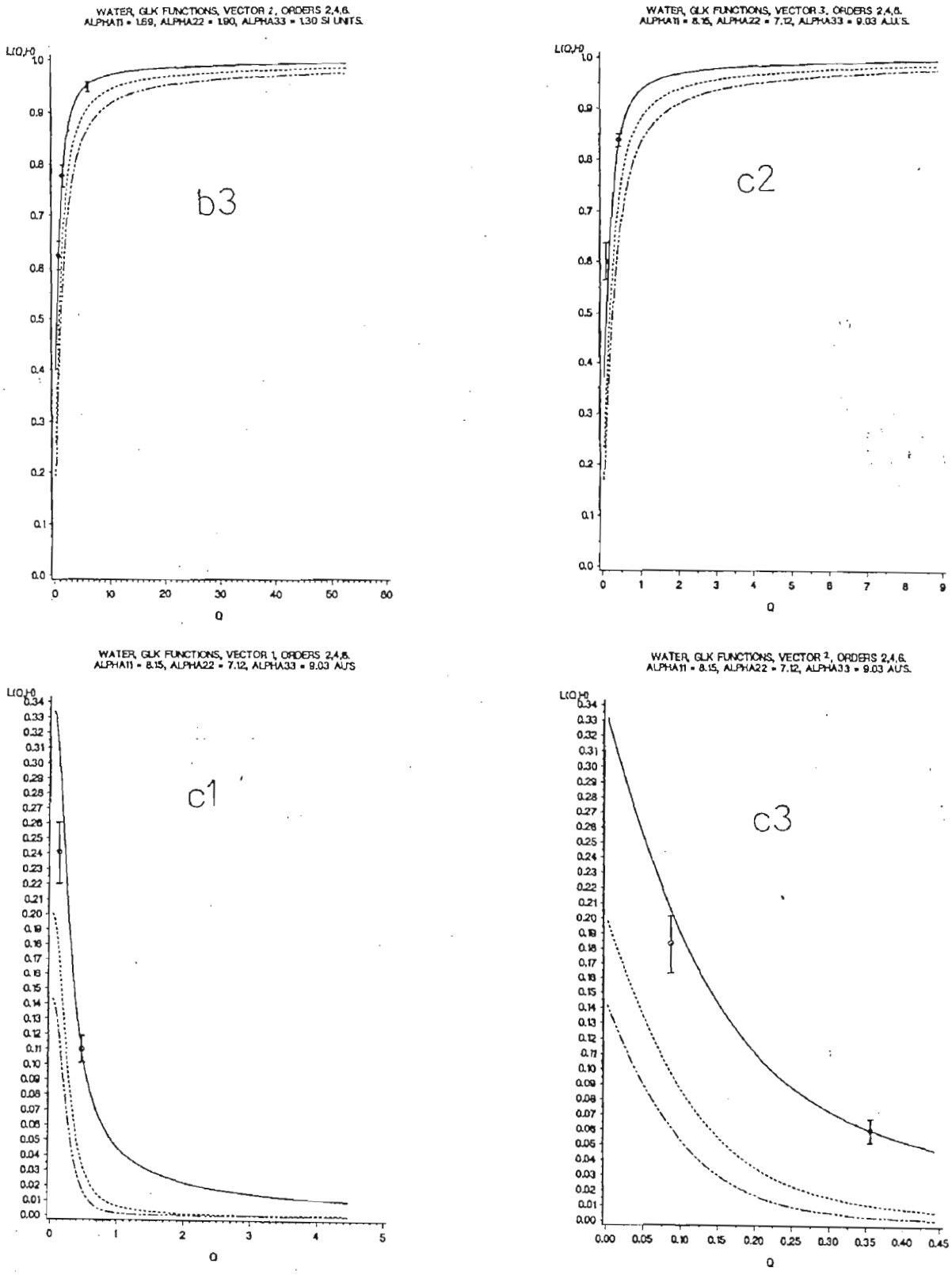
WATER, GLK FUNCTIONS, VECTOR 2, ORDERS 2,4,6.
ALPHA11 = 1.59, ALPHA22 = 1.90, ALPHA33 = 1.30 SI UNITS.
L(Q,J=0
Q
b3
WATER, GLK FUNCTIONS, VECTOR 3, ORDERS 2,4,6.
ALPHA11 = 8.15, ALPHA22 = 7.12, ALPHA33 = 9.03 A.U.'S.
L(Q,J=0
Q
c2
WATER, GLK FUNCTIONS, VECTOR 1, ORDERS 2,4,6.
ALPHA11 = 8.15, ALPHA22 = 7.12, ALPHA33 = 9.03 AU'S
L(Q,J=0
Q
c1
WATER, GLK FUNCTIONS, VECTOR 2, ORDERS 2,4,6.
ALPHA11 = 8.15, ALPHA22 = 7.12, ALPHA33 = 9.03 AU'S.
L(Q,J=0
Q
c3

Fig. 1 (cont.).

and again this is reproduced successfully by FMD. For $|\delta/\gamma| \gg 1$ this blip disappears, and the function $\langle e_X^n \rangle$ is monotonically decreasing.

These results show that:

(1) The sign of the anisotropy of polarisability of the water molecule can be determined from an accurate experimental measurement of the three GLKs described already, possibly with contemporary femtosecond transient optical Kerr effect apparatus [5].

(2) FMD is in detailed agreement with the analytical theory on GLKs.

5. Time resolution of optical Kerr effect rise transients

The time resolution on the femtosecond level of the optical Kerr effect has been achieved [5] in a range of molecular liquids by Kenney-Wallace and co-workers. The data are in the form of rise transients of probe optical absorption as a pump pulse is passed through the ensemble. These data can be related to our GLKs through the birefringence of the optical Kerr effect, which is in turn related to the observable changes in power absorption coefficient [5] through the Kramers–Kronig equations. The birefringence function is given analytically in terms of generalised Langevin–Kielich functions and generalised O'Konski functions, Φ, as described in section 6.

It is possible therefore, using a numerical iterative scheme, for example, to determine the anisotropy of polarisability from the rise transient experimental data [5]. Furthermore, FMD gives the time resolution of the rise transient as illustrated in fig. 4 using the apparently conflicting literature data sets of table 1. Figure 4 shows that the time resolved transients are markedly different for each data set at fixed pump laser equivalent potential energy, obtained by intergrating the torque over configuration space in the FMD algorithm. For the Zeiss/Meath estimate [33] there are no rise transient oscillations [16, 17] known from diffusion theory [17] to be due to specific non-linearities in the molecular dynamics. The presence of these oscillations is observed clearly (fig. 4), however, using the data given by Khanarian and Ken [34] and the ab initio computation of Van Hemert and Blom [35] for constant applied pump laser intensity in the simulation for all three cases. This shows clearly the dependence of the rise transient on the precise details of the anisotropy of polarisability for given pump laser intensity.

It is concluded that the details of the time dependence of the optical Kerr effect rise transient are intricate functions of the anisotropy of polarisability at a given pump laser intensity. It would be of interest to attempt to observe such oscillations experimentally [5].

6. Generalised Langevin–Kielich, Φ, R, and K functions

In this section we evaluate the optically induced orientational anisotropy leading to the optical Kerr effect for molecules with arbitrary symmetry. Applying the molecular theory [2] to an isotropic medium acted on by an intense, linearly polarised, optical beam with electric field strength E we have the birefringence due to pure reorientational processes in the form

$$n_{\parallel} - n_{\perp} = \frac{n\rho}{2\epsilon_0}\left(\frac{n^2+2}{3n}\right)^2 \gamma\left(\Phi(q,h) + \frac{3}{2}\frac{h}{q}R(q,h)\right)$$

$$\equiv \frac{n\rho}{2\epsilon_0}\left(\frac{n^2+2}{3n}\right)^2 \gamma K(q,h)\,, \tag{18}$$

where $n_{\parallel}$ and $n_{\perp}$ are the refractive indices for a probe beam with electric field vibrating parallel and perpendicular to E, respectively, n is the refractive index with the external field, ρ the molecular number density, and the orientational functions

$$\Phi(q, h) = \tfrac{1}{2}(3L_2(q, h) - 1) \tag{19}$$

$$R(q, h) = L_2^{(1)}(q, h) - L_2^{(2)}(q, h) \tag{20}$$

are given by GLK functions (9)–(11). The function Φ is appropriately referred to as the generalised Langevin–O'Konski function, because for $h = 0$, it reduces to the O'Konski function $\Phi(q)$ [28–32, 42]. These sets of curves are presented in figs. 2 and 3, which are reference curves for the general asymmetric top for the optical Kerr effect and related phenomena [2, 31]. These curves are sensitive to h/q, and form a rich variety of potentially observable behaviour under the right conditions, for example in macromolecules with the techniques [2, 38] of non-linear dielectric spectroscopy as well as with those of the optical and electric Kerr effects. In the isotropic phases of liquid crystals of asymmetric top molecules, the birefringence function can also be saturated [24].

In the particular case of water, using the data sets of table 1, large differences in the birefringence functions $K(q, h)$ versus $|q|$ are easily seen in fig. 5. These differences originate in insufficient state of the art experimental precision and somewhat conflicting frame definitions in the literature data, amounting to the uncertainty even in the sign of the anisotropy δ of the water molecule. We note that Khanarian and Kent [34] appear to have defined the polarisability components in axes 2 and 3 oppositely to Zeiss and Meath [33] and Van Hemert and Blom [35]. For the simulation and theory of this paper, the data of table 1 were used throughout. A simulation of the rise transients of the birefringence function (18) is given in fig. 6 under the same conditions as illustrated in fig. 5, showing large differences in details of time resolution as a function of anisotropy of polarisability on the femtosecond time scale now accessible experimentally.

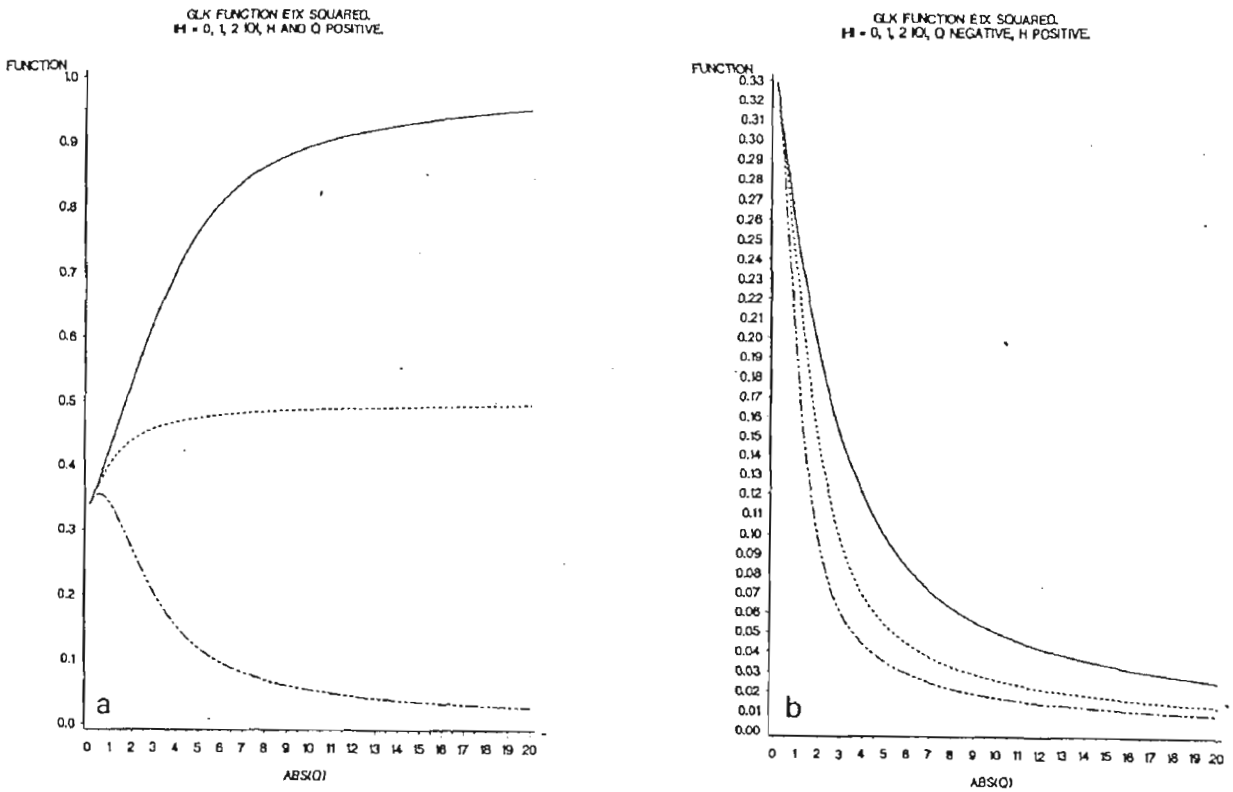

Fig. 2. GLK functions from eq. (9) for vector $\langle e_{1x}^2 \rangle$. Presented as master curves as a function of $|q|$. ——, $h/q = 0$; - - -, $h/q = 1$; – · · – · · –, $h/q = 2$. (a) h and q positive; or q positive, h negative; (b) q negative, h positive; or q and h negative.

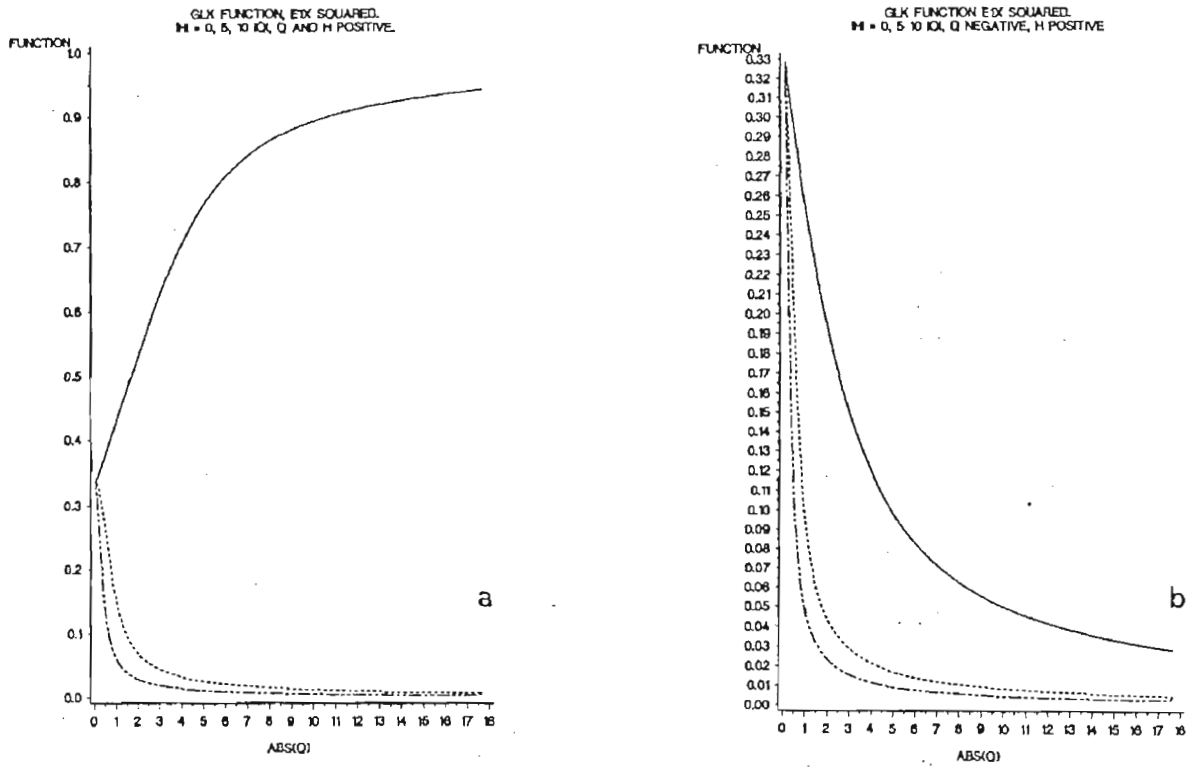

Fig. 3. As for fig. 2; ——, $h/q = 0$; ----, $h/q = 5$; – · · – · · –, $h/q = 10$.

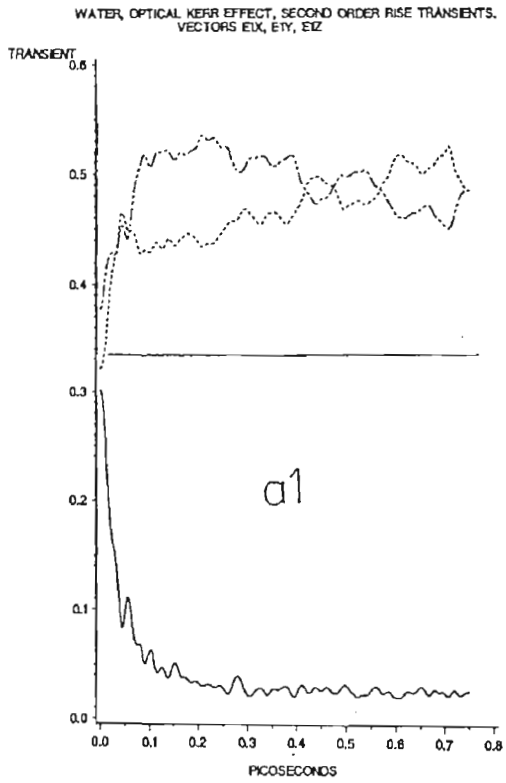

Fig. 4. Time resolution of transients from data sets (a), (b) and (c), simulated by FMD with equivalent laser potential energy of 2.0 kJ/mol. ——, $X = \langle e_{iX}^n \rangle$; ----, $Y = \langle e_{iY}^n \rangle$; – · · –, $Z = \langle e_{iZ}^n \rangle$; $i = 1, 3, 2$, respectively, $n = 2$.

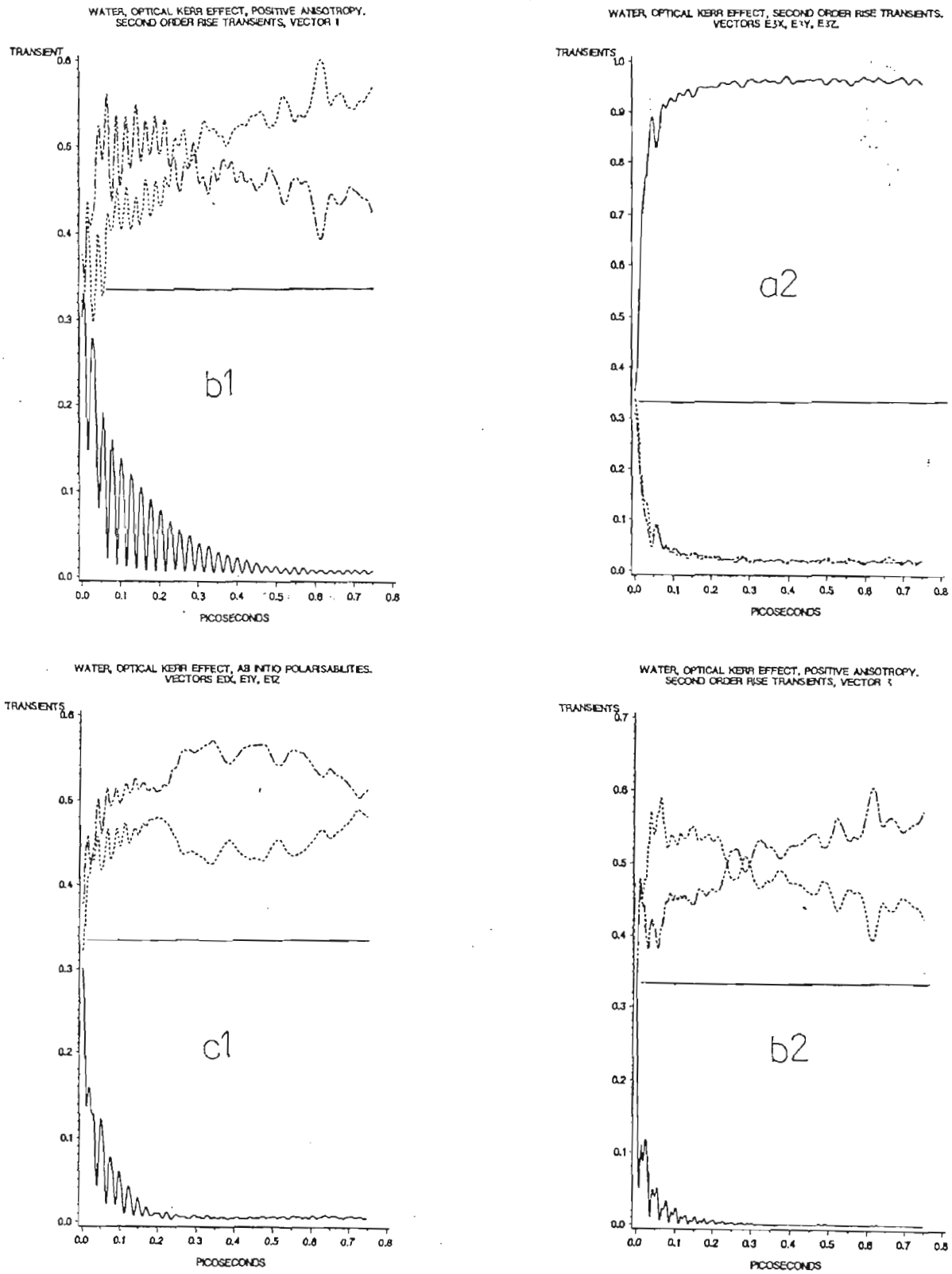
WATER, OPTICAL KERR EFFECT, POSITIVE ANISOTROPY.
SECOND ORDER RISE TRANSIENTS, VECTOR I
TRANSIENT
b1
PICOSECONDS
WATER, OPTICAL KERR EFFECT, SECOND ORDER RISE TRANSIENTS.
VECTORS E3X, E3Y, E3Z
TRANSIENTS
a2
PICOSECONDS
WATER, OPTICAL KERR EFFECT, AB INITIO POLARISABILITIES.
VECTORS E0X, E0Y, E0Z
TRANSIENTS
c1
PICOSECONDS
WATER, OPTICAL KERR EFFECT, POSITIVE ANISOTROPY.
SECOND ORDER RISE TRANSIENTS, VECTOR
TRANSIENTS
b2
PICOSECONDS

Fig. 4 (cont.).

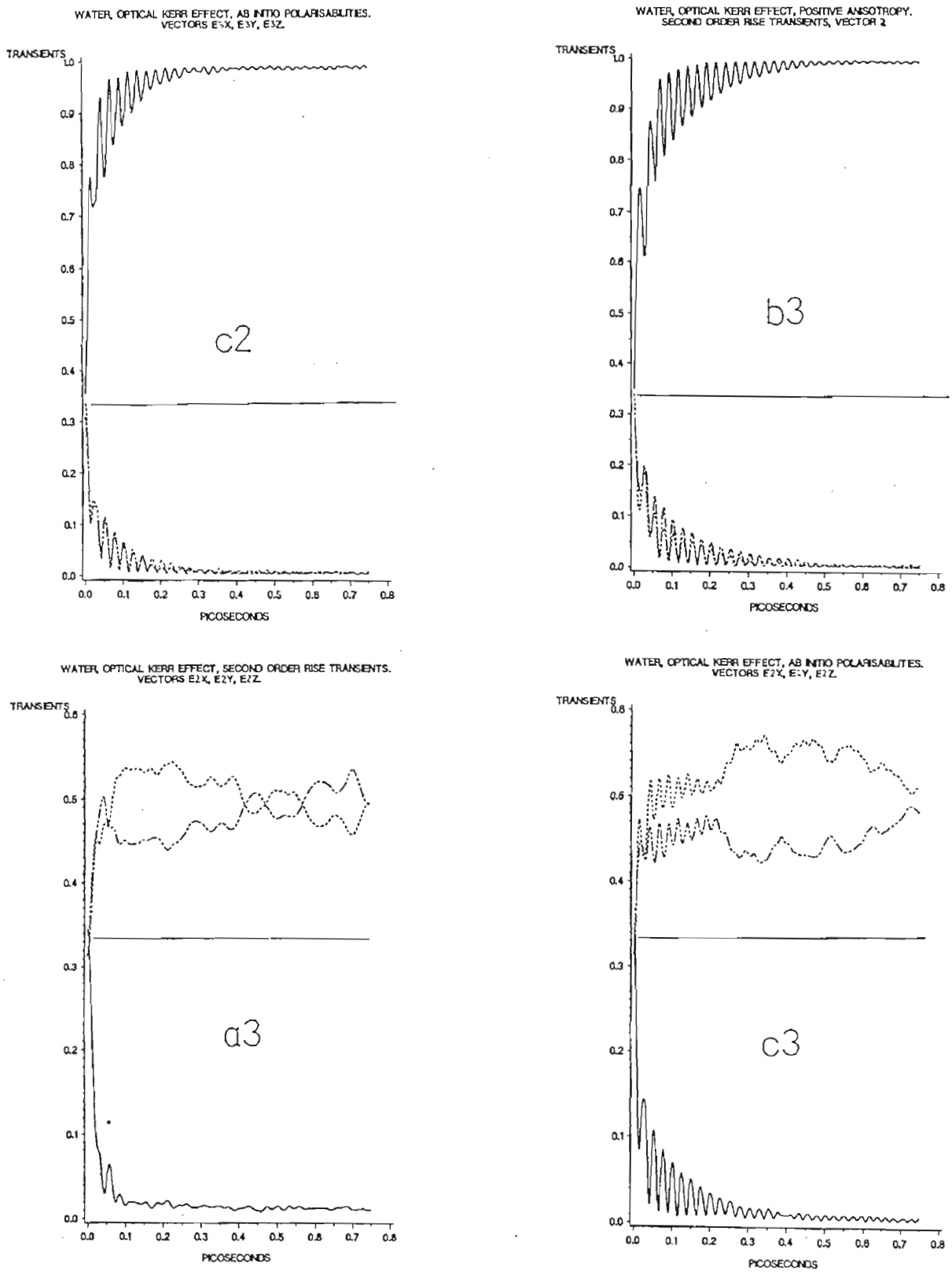
WATER, OPTICAL KERR EFFECT, AB INITIO POLARISABILITIES.
VECTORS E3X, E3Y, E3Z.
TRANSIENTS
c2
PICOSECONDS
WATER, OPTICAL KERR EFFECT, POSITIVE ANISOTROPY.
SECOND ORDER RISE TRANSIENTS, VECTOR 2
TRANSIENTS
b3
PICOSECONDS
WATER, OPTICAL KERR EFFECT, SECOND ORDER RISE TRANSIENTS.
VECTORS E1X, E1Y, E1Z.
TRANSIENTS
a3
PICOSECONDS
WATER, OPTICAL KERR EFFECT, AB INITIO POLARISABILITIES.
VECTORS E2X, E2Y, E2Z.
TRANSIENTS
c3
PICOSECONDS

Fig. 4 (cont.).

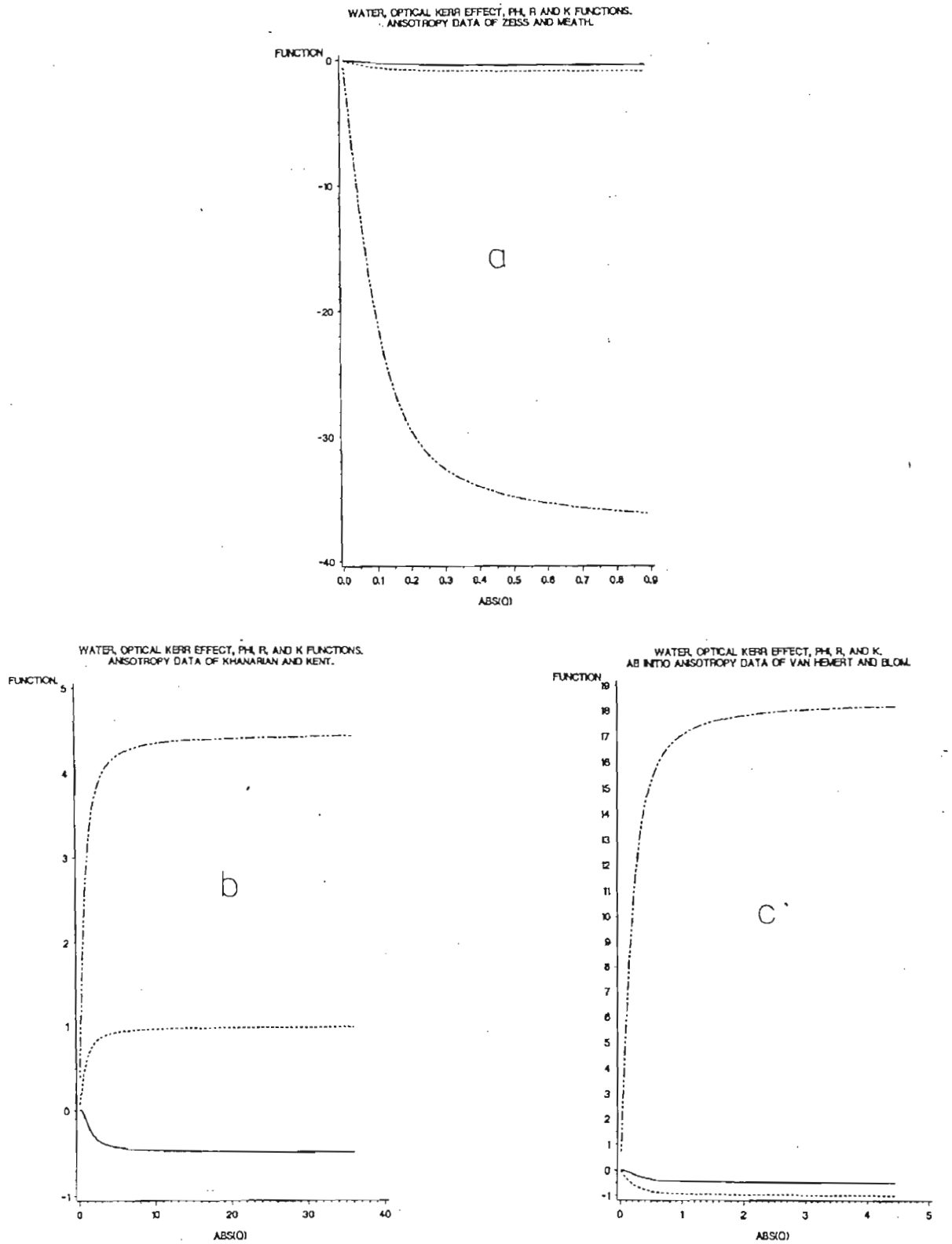

Fig. 5. Comparison of optical Kerr effect in water for the three data sets of table 1: ———, Φ function; ---, R function; – · · –, K function. (a) Zeiss and Meath [33]; (b) Khanarian and Kent [34]; (c) Van Hemert and Blom [35]. Plotted vs. $|q|$.

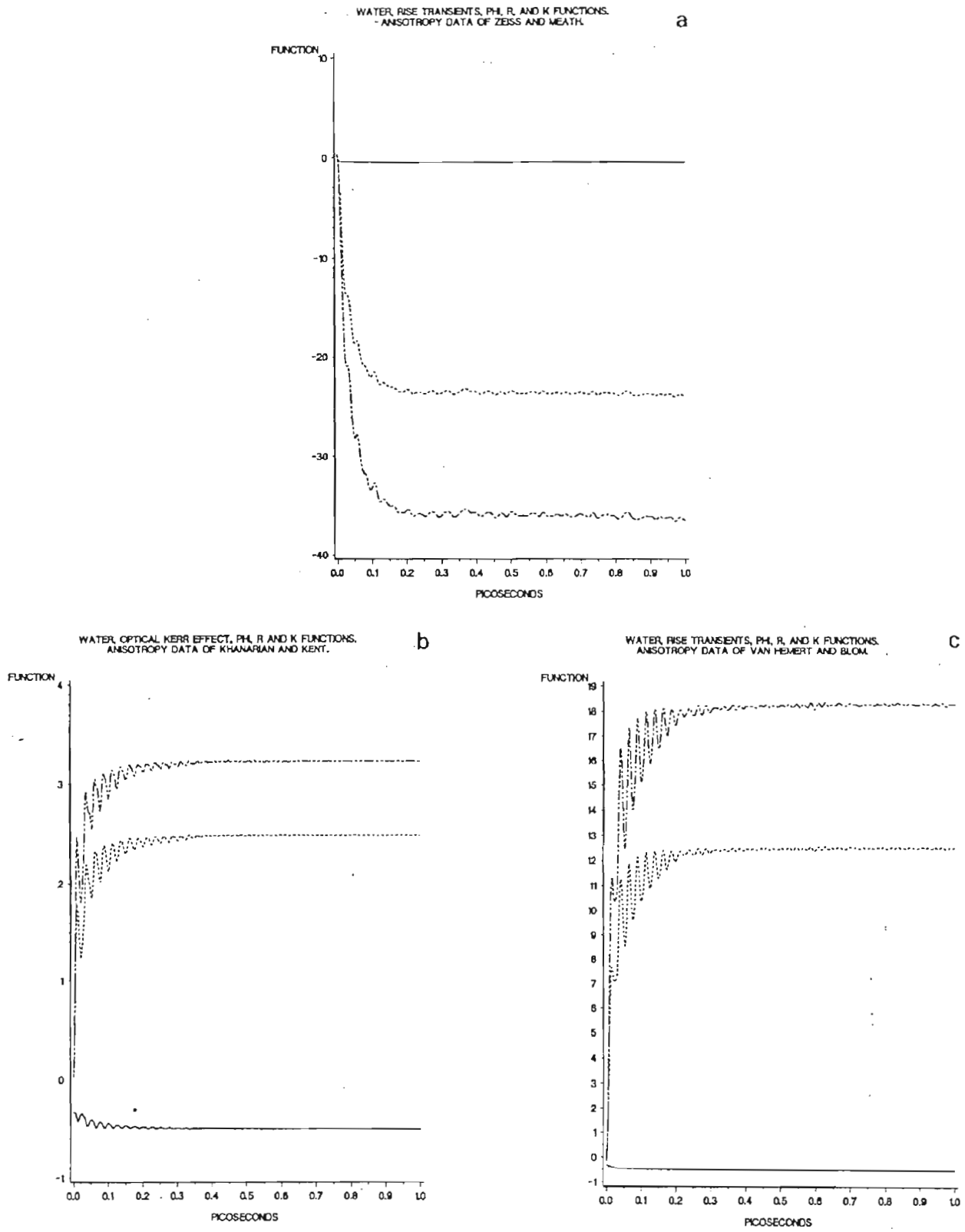

Fig. 6. As for fig. 4, time resolution of rise transients. ——, Φ; ---, R; and –·–·–, K for the data sets of table 1: (a) Zeiss and Meath [33]; (b) Khanarian and Kent [34]; (c) Van Hemert and Blom [35]. Plotted vs. picoseconds.

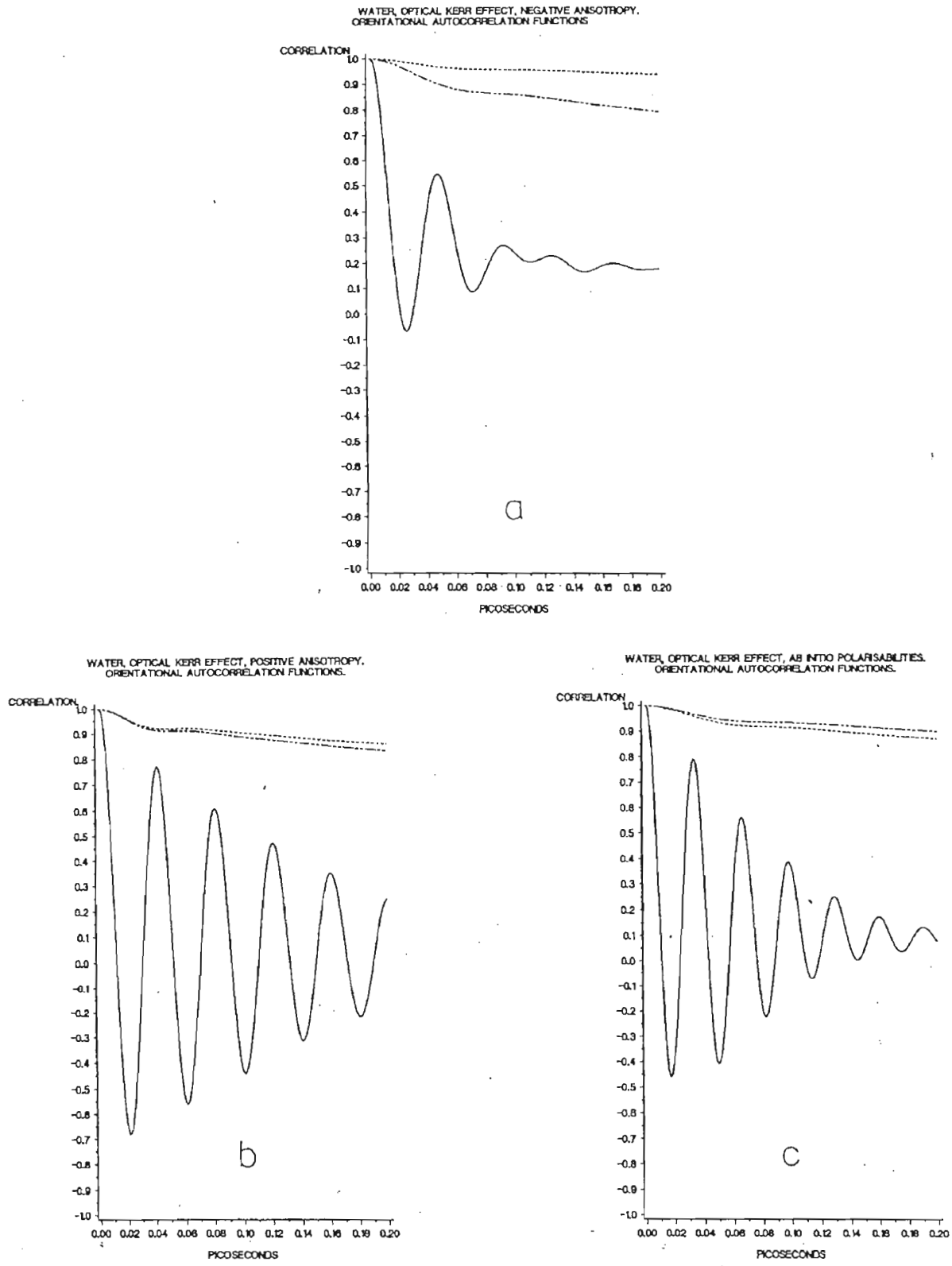

Fig. 7. As for fig. 4, orientational autocorrelation functions in the post transient steady state for data sets (a), (b) and (c) of table 1. Functions C_{ij}; ——, $i = j = X$; - - - $i = j = Y$; – · · –, $i = j = Z$.

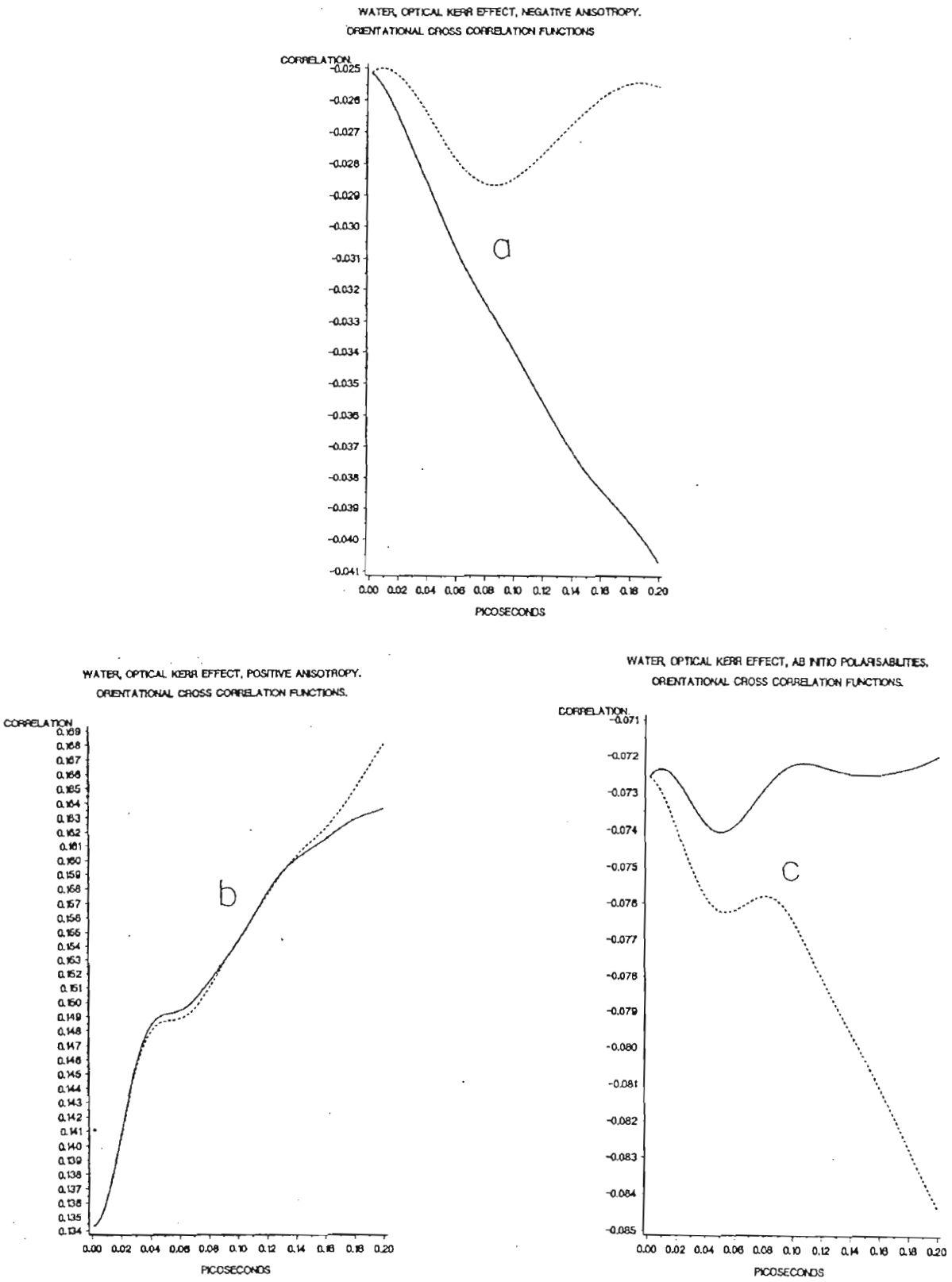

Fig. 8. As for fig. 7, orientational cross correlation functions, C_{ij}; ———, $i = X$, $j = Y$; ---, $i = Y$, $j = X$.

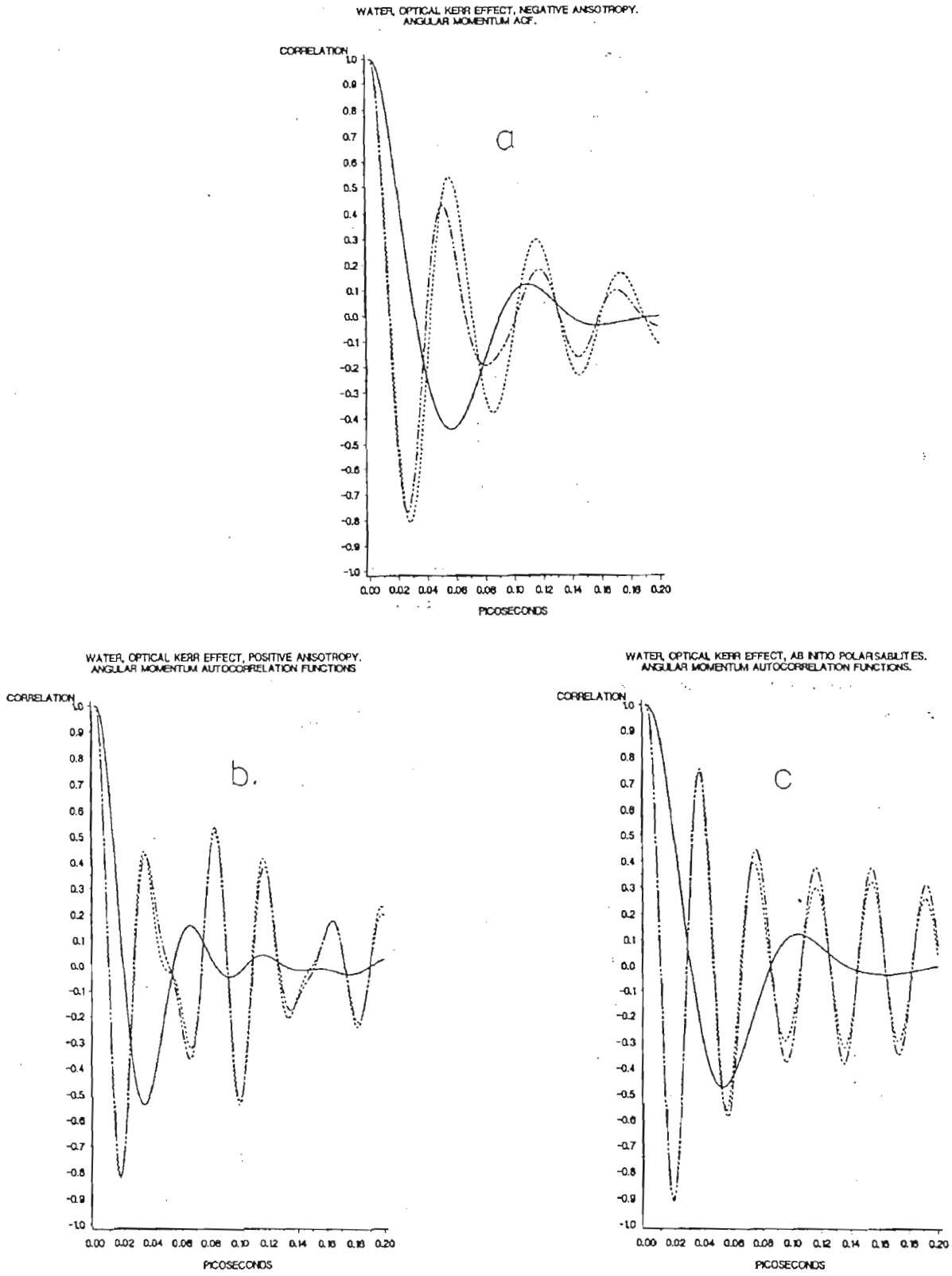

Fig. 9. As for fig. 7, angular momentum autocorrelation functions.

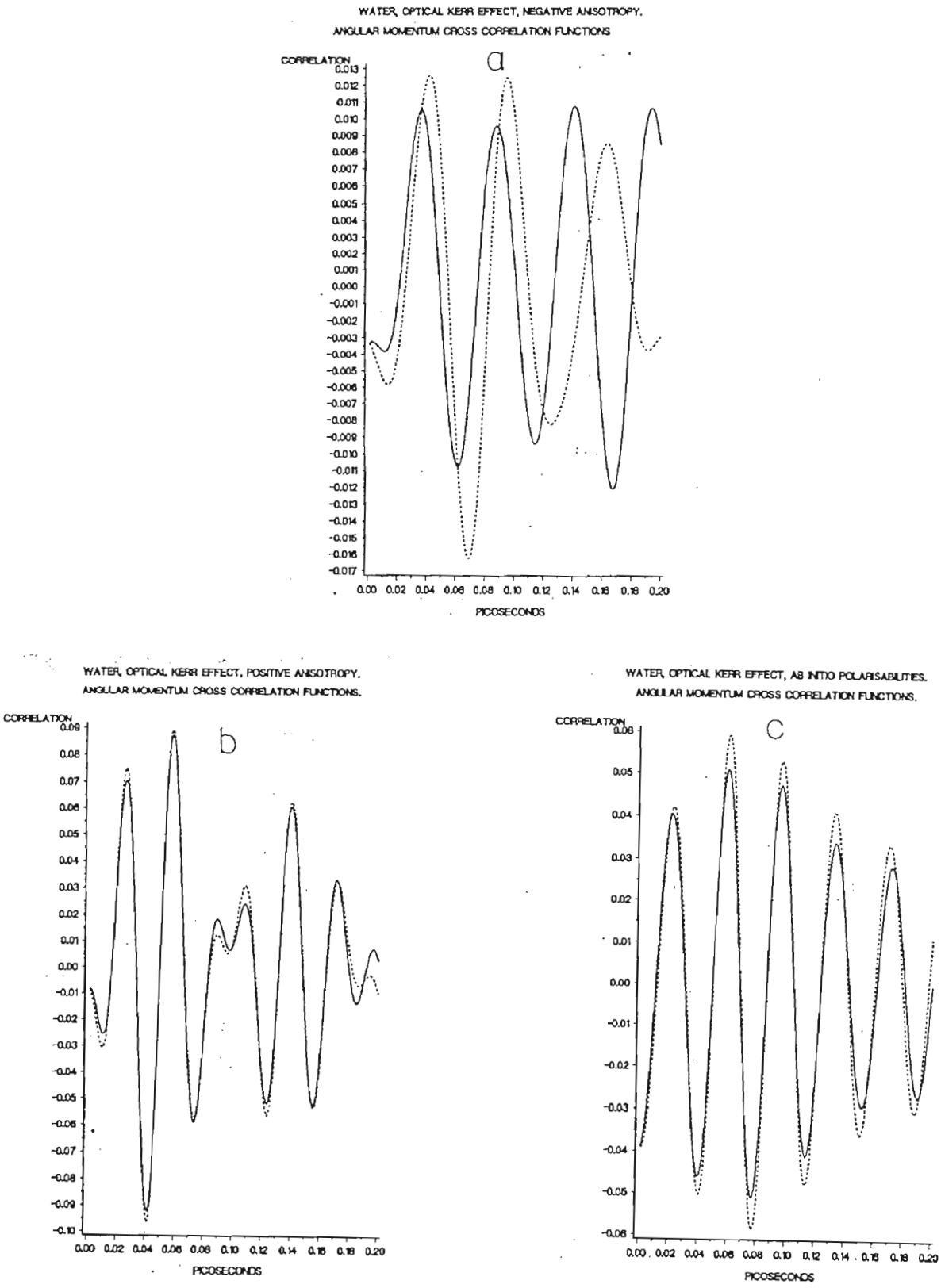

Fig. 10. As for fig. 8, angular momentum cross-correlation functions.

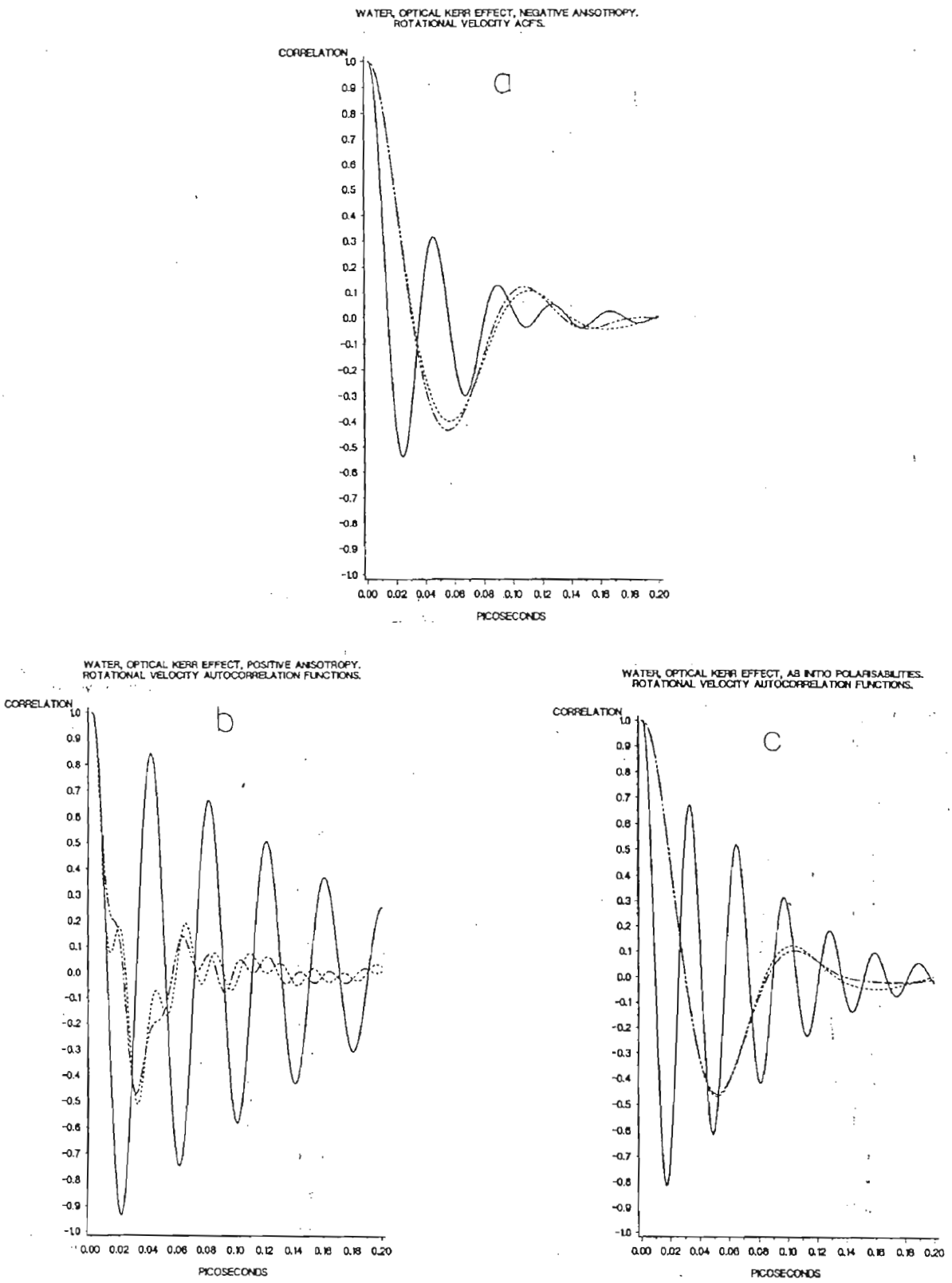

Fig. 11. As for fig. 7, rotational velocity autocorrelation functions.

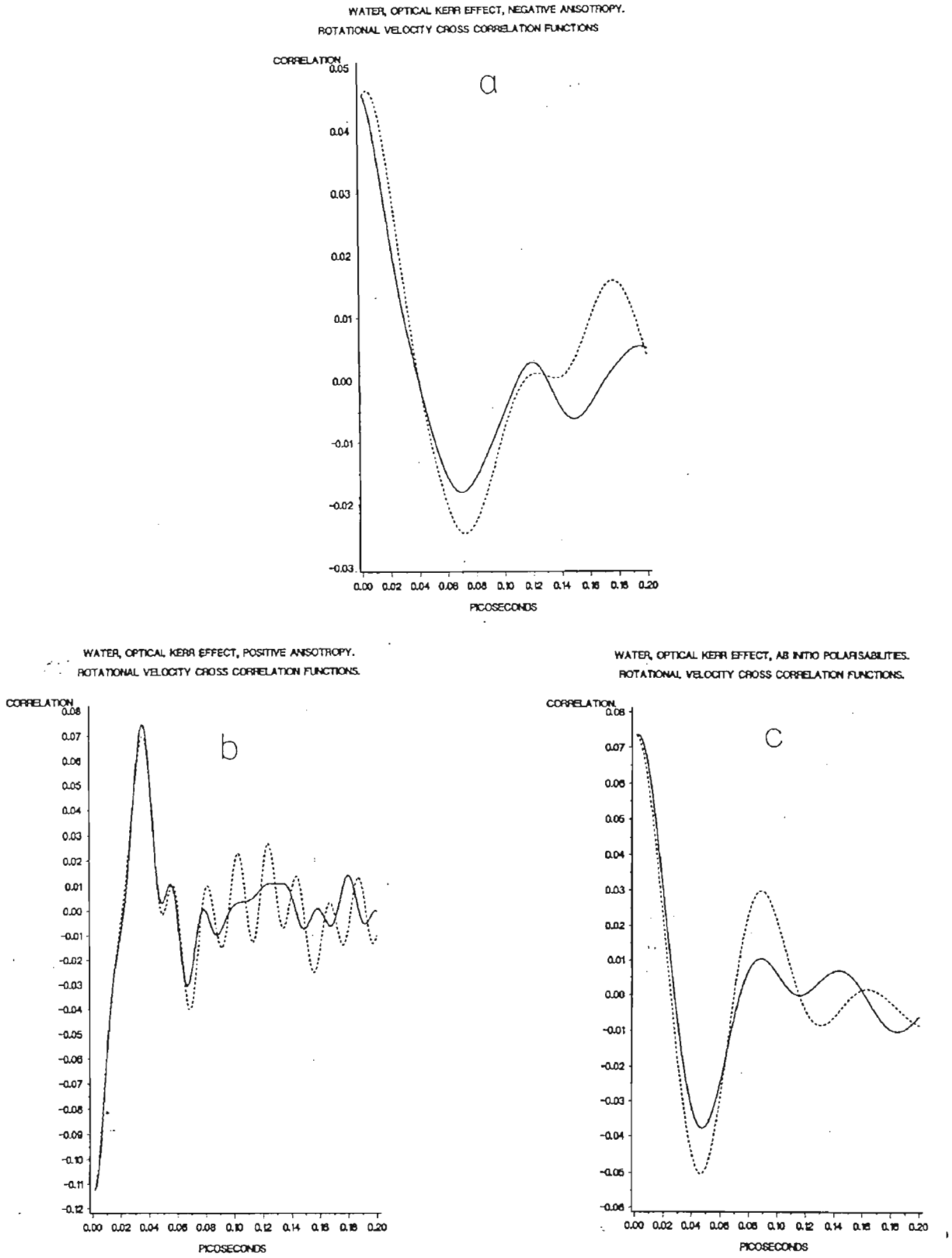

Fig. 12. As for fig. 8, rotational velocity cross-correlation functions.

7. Laser-on time correlation functions

Finally, we report that in the laser field applied steady state reached by the rise transient at a given pump laser intensity, a data bank of time correlation functions was accumulated to investigate in detail the field-on statistical dynamics by FMD. The correlation functions were also observed to be markedly dependent on which data set of table 1 was used, and this is exemplified in figs. 7–12 for the orientational correlation functions

$$C_{1ij}(t) = \frac{\langle e_{1i}(t)e_{1j}(0)\rangle}{\langle e_{1i}^2\rangle^{1/2}\langle e_{1j}^2\rangle^{1/2}}\,, \tag{21}$$

the rotational velocity correlation functions [3]

$$C_{2ij}(t) = \frac{\langle \dot{e}_{1i}(t)\dot{e}_{1j}(0)\rangle}{\langle \dot{e}_{1i}^2\rangle^{1/2}\langle \dot{e}_{1j}^2\rangle^{1/2}}\,, \tag{22}$$

and the angular momentum correlation functions

$$C_{3ij}(t) = \frac{\langle J_i(t)J_j(0)\rangle}{\langle J_i^2\rangle^{1/2}\langle J_j^2\rangle^{1/2}}\,. \tag{23}$$

Off diagonal components (cross-correlation functions) were found (figs. 8, 10, 12), to change sign with the anisotropy of polarisability δ. Patterns of laser induced oscillations for the autocorrelation functions, and the extent of anisotropy in their time development, are all greatly affected by which data set of table 1 is accepted as the most accurate.

The Fourier transform of the rotational velocity autocorrelation function [1] is the far infrared power absorption coefficient, and were it possible to observe this spectrum in the presence of a pump laser pulse, FMD as used in this paper shows that it would give information on the molecular dynamics of the optical Kerr effect in the laser on steady state, and specifically on the anisotropy of polarisability.

Acknowledgements

MWE and SW thank Professor Dr. Georges Wagnière for an invitation to the University of Zurich as Guests of the University. The Swiss NSF is thanked for the award of Senior Visiting Fellowships. ETH Zurich is acknowledged for a major grant of computer time on the IBM 3090 supercomputer on which this work was carried out. Dr. Laura J. Evans is thanked for invaluable help with the SAS plotting facility of the Irchel mainframe, used to build up the data banks.

References

[1] M.W. Evans, in: Advances in Chemical Physics, eds. I. Prigogine and S.A. Rice, Vol. 81 (Wiley Interscience, New York) in press.
[2] S. Kielich, in: Dielectric and Related Molecular Processes Vol. 1, M. Davies, senior rep. (Chem. Soc., London, 1972).
[3] M.W. Evans, J. Chem. Phys. 76 (1982) 5473, 5480.
[4] M.W. Evans, J. Chem. Phys. 77 (1982) 4632; 78 (1983) 925, 5403.
[5] C. Kalpouzos, D. McMorrow, W.T. Lotshaw and G.A. Kenney-Wallace, Chem. Phys. Lett. 150 (1988) 138.

[6] M.W. Evans, P. Grigolini, G. Pastori, I. Prigogine and S.A. Rice, eds., Advances in Chemical Physics, Vol. 62 (Wiley Interscience, New York, 1985).
[7] J. Jortner, R.D. Levine, I. Prigogine and S.A. Rice, eds., Advances in Chemical Physics, Vol. 47 (Wiley Interscience, New York, 1981).
[8] M.W. Evans, Phys. Scripta 30 (1984) 91.
[9] E. Clementi, ed., MOTECC 89 and 90 (Escom, Reidel).
[10] M.W. Evans, G.C. Lie and E. Clementi, Chem. Phys. Lett. 138 (1987) 149.
[11] M.W. Evans, G.C. Lie and E. Clementi, J. Chem. Phys. 87 (1987) 6040.
[12] G. Wagnière, Phys. Rev. A 40 (1989) 2437.
[13] D.C. Hanna, M.A. Yuratich and D. Cotter, in: Non-Linear Optics of Free Atoms and Molecules (Springer, New York, 1979).
[14] M.W. Evans and G. Wagnière, Phys. Rev. A 42 (1990) 6732.
[15] P. Grigolini, in ref. [6].
[16] M.W. Evans, G.C. Lie and E. Clementi, Phys. Lett. A 130 (1988) 289.
[17] W.T. Coffey, in: Advances in Chemical Physics, eds. M.W. Evans, I. Prigogine and S.A. Rice, Vol. 83 (Wiley Interscience, New York, 1985).
[18] L.D. Barron, Molecular Light Scattering and Optical Activity (Cambridge University Press, 1982).
[19] G. Mayer and F. Gires, Compt. Rend. Acad. Sci. 258 (1964) 2039.
[20] M. Paillette, ibid. 262 (1966) 264; 266 (1968) 920; Ann. Phys. 4 (1969) 671.
[21] S. Kielich, J.R. Lalannes and F.B. Martin, J. Phys. (Paris) 33 (1972) 191.
[22] Z. Blaszczak, A. Dobek and A. Patkowski, Acta Phys. Pol. A 44A (1973) 151; 45 (1974) 269.
[23] K. Sala and M.C. Richardson, J. Appl. Phys. 49 (1978) 2268.
[24] H.J. Coles and B.R. Jennings, Mol. Phys. 31 (1976) 570.
[25] A.D. Buckingham, Proc. Phys. Soc. B 69 (1956) 444.
[26] M.W. Evans, K.N. Swamy, K. Refson, G.C. Lie and E. Clementi, Phys. Rev. A 36 (1988) 3935.
[27] M.W. Evans, G.C. Lie and E. Clementi, J. Chem. Phys. 88 (1988) 5157.
[28] S. Kielich, Acta Phys. Pol. 36 (1969) 621; A 37 (1970) 447, 719.
[29] S. Kielich, J. Colloid Interface Sci. 34 (1970) 228.
[30] S. Woźniak, Mol. Phys. 59 (1986) 421.
[31] S. Woźniak, J. Chem. Phys. 85 (1986) 4217; and in press (1991).
[32] S. Woźniak, Phys. Lett. A 148 (1990) 188; 119 (1986) 256.
[33] G.D. Zeiss and W.J. Meath, Mol. Phys. 30 (1975) 161.
[34] G. Khanarian and L. Kent, J. Chem. Soc. Faraday Trans. II 77 (1981) 495.
[35] M.C. van Hemert and C.E. Blom, Mol. Phys. 43 (1981) 229.
[36] M.S. Beevers and G. Khanarian, Aust. J. Chem. 33 (1980) 2585.
[37] W.F. Murphy, J. Chem. Phys. 67 (1977) 5877.
[38] R.K. Khanno, E. Dempsey and G. Parry Jones, Chem. Phys. Lett. 53 (1978) 542.
[39] E.A. Moelwyn Hughes, Physical Chemistry (Pergamon, Oxford, 1964), pp. 384, 473.
[40] IBM ESSL Library, routine DGLNQ2.
[41] S. Kielich, Nonlinear Molecular Optics (Nauka, Moscow, 1981).
[42] C.T. O'Konski, K. Yoshioka and W.H. Orttung, J. Chem. Phys. 63 (1959) 1558.